

www.aem-journal.com

Additive Manufacturing of Sandwich-Structured Conductors for Applications in Flexible and Stretchable Electronics

Xiaowei Yu, Xiangtao Gong, Chinmoy Podder, Brandon Ludwig, I-Meng Chen, Wan Shou, Alexis Alvidrez, Genda Chen, Xian Huang, and Heng Pan*

Additive manufacturing methods have shown great potentials to substitute the costly and time-consuming conventional subtractive methods in the processing of electronically conductive materials for applications in flexible and stretchable electronics. Herein, additive manufacturing of highly conductive, sandwichstructured conductors with high-temperature processibility and versatility in applicable substrates is reported. The sandwich-structured conductors with silver nanoparticles (Ag NPs) as electronic conductors and polyimide (PI) as encapsulation are layer-by-layer deposited by aerosol printing into PI/Ag/PI composites. A high annealing temperature of 250 °C contributes to the high electronic conductivity of the Ag layer at 1.14×10^7 S m⁻¹, which is in the same order of magnitude to the conductivity of bulk Ag at 6.3×10^7 S m⁻¹. The high annealing temperature also significantly improves the interfacial bonding between the Ag and PI layers. For applications in flexible and stretchable electronics, the sandwich-structured conductors are transferrable to various substrates through a thiol-epoxy bonding process, including polystyrene (PS), polyethylene terephthalate (PET), Kapton, and polydimethylsiloxane (PDMS) thin films. The sandwich-structured conductors transferred to flexible and stretchable substrates exhibit highly retained electronic conductivity under deformations such as bending and stretching.

1. Introduction

In the last decade, polymer thin film-based flexible and stretchable electronics with a soft and deformable nature have drawn tremendous interests in the scientific community.^[1,2] Various applicable fields, such as wearable electronics,^[3,4] soft robotics,^[5,6] biomedical monitoring, and therapeutic devices,^[7,8]

are emerging, underscoring the necessity of developing the low-cost and large-scale manufacturing process for these devices. Currently, conventional microfabrication methods are playing a dominant role in the manufacturing of these devices, which involve expensive vacuum-based deposition and time-consuming subtractive etching processes.^[9,10] As alternatives, additive printing techniques such as inkjet printing, [11,12] aerosol printing, [13–16] and electrohydrodynamic printing^[17,18] with atmospheric-processing capabilities have shown great potentials in the future direction toward the low-cost and largescale manufacturing of flexible and stretchable electronics.

The printing of electronically conductive materials is the essential step in the additive manufacturing of flexible and stretchable electronics. Despite the significant progress of printed conductors with carbon-based nanomaterials^[19,20] and conductive polymers,^[12,21] their electronic conductivity is significantly lower (usually in several orders of magnitude) compared

with the metallic materials used in conventional electronics. Contacts and interconnects requiring higher conductivity are usually realized through the printing of highly conductive metal ink with metallic nanoparticles (NPs). These NPs can be sintered into electronically conductive networks during the postprocess annealing. [22,23] However, there usually exists a trade-off between the electronic conductivity of these NP-based conductors and the

X. Yu, X. Gong, C. Podder, B. Ludwig, I.-M. Chen, W. Shou, H. Pan Department of Mechanical and Aerospace Engineering Missouri University of Science and Technology Rolla, MO 65401, USA E-mail: hp5c7@mst.edu

X. Gong, C. Podder, H. Pan J. Mike Walker '66 Department of Mechanical Engineering Texas A&M University College Station, TX 77843, USA

The ORCID identification number(s) for the author(s) of this article can be found under https://doi.org/10.1002/adem.202100286.

DOI: 10.1002/adem.202100286

A. Alvidrez Department of Mechanical Engineering The University of Texas at El Paso El Paso, TX 79968, USA

G. Chen
Department of Civil, Architectural and Environmental Engineering
Missouri University of Science and Technology
Rolla, MO 65401, USA

X. Huang Department of Biomedical Engineering Tianjin University Tianjin 300072, China

www.aem-journal.com

annealing temperature, [24-26] which is limited by the glass transition temperature (T_o) of the polymeric substrates. [27,28] Except for polyimide (PI) as a well-known thermally stable polymer, [29,30] printed NPs-based conductors on other polymeric substrates such as polyethylene terephthalate (PET) usually cannot be annealed at temperatures higher than 150°C,[31-33] resulting in insufficient sintering of the NPs and unsatisfactory device performance.[34] In addition, additive manufacturing of conductors on elastomeric substrates such as polydimethylsiloxane (PDMS) has been reported in several works by direct printing of NP-based conductive inks, as shown in Table S1.[35-40] Nevertheless, the processibilities are limited due to issues related to the material properties of the substrate, such as poor compatibility with the solvents in the printable inks[41,42] and the mechanical failure induced by thermal expansion coefficient mismatch^[35,37] between the substrate and printed materials.

In this work, additive manufacturing of highly conductive, sandwich-structured NP-based conductors is reported. The printed conductors are processable at a high temperature of 250 °C and are transferrable to various substrates through a thiol—epoxy bonding process, [43,44] including polystyrene (PS), PET, Kapton, and PDMS thin films for applications in flexible and stretchable electronics. The additive manufacturing process including the layer-by-layer aerosol printing of the sandwich-structured conductors and the subsequent substrate-transferring step is shown in **Figure 1**a, with photographs of an array of sandwich-structured conductors on donor (glass), intermediate

(water-soluble tape), and target (PDMS) substrates in Figure 1b, demonstrating the large-scale manufacturing capability. The Ag layer annealed at 250 °C exhibits high electronic conductivity of 1.14×10^7 S m⁻¹, which is in the same order of magnitude to the conductivity of bulk silver at 6.3×10^7 S m^{-1[25]} and is sufficiently high for serving as the contacts and interconnects in most applications. The high temperature used during postprocess annealing also has an important impact on the improved interfacial bonding between the Ag and PI layers. The sandwich-structured conductors transferred to flexible and stretchable substrates exhibit highly retained electronic conductivity under deformations such as bending and stretching. The proposed additive manufacturing method could serve as a potential route for the fabrication of conductors in flexible and stretchable electronics with versatility in applicable substrates and high-temperature processibility to achieve desired device performance.

2. Results and Discussion

For the additive manufacturing of sandwich-structured conductors, the PI layer and Ag layer were deposited by aerosol printing with Collison nebulizer (Figure 2a) and ultrasonic particle generator (Figure 2b), respectively. During the layer-by-layer printing, a bottom-view coaxial microscope (Figure 2c) was used to ensure the alignment of each layer. The layer-by-layer printability

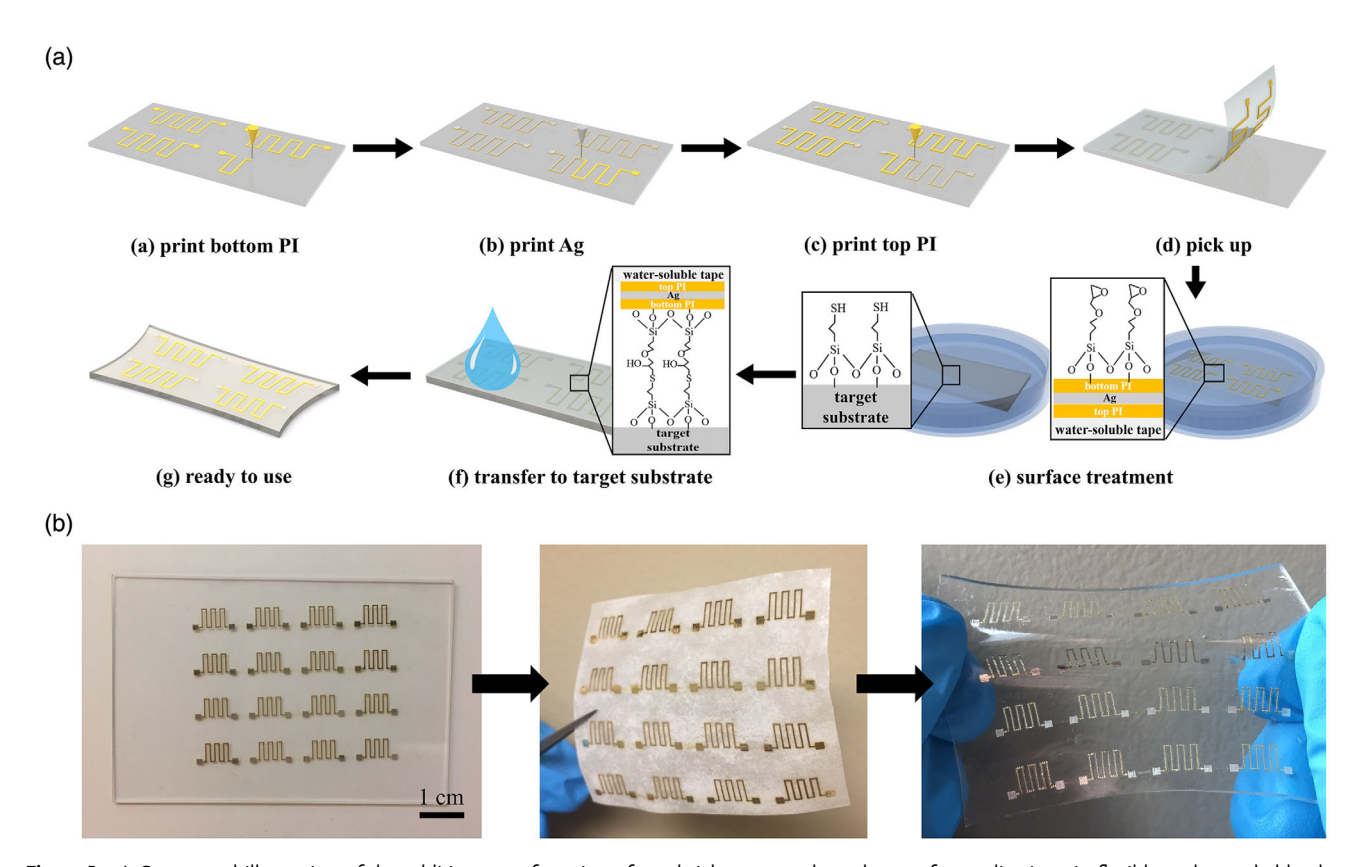


Figure 1. a) Conceptual illustration of the additive manufacturing of sandwich-structured conductors for applications in flexible and stretchable electronics. b) Photographs of an array of sandwich-structured conductors on donor, intermediate, and target substrates.

www.advancedsciencenews.com www.aem-journal.com

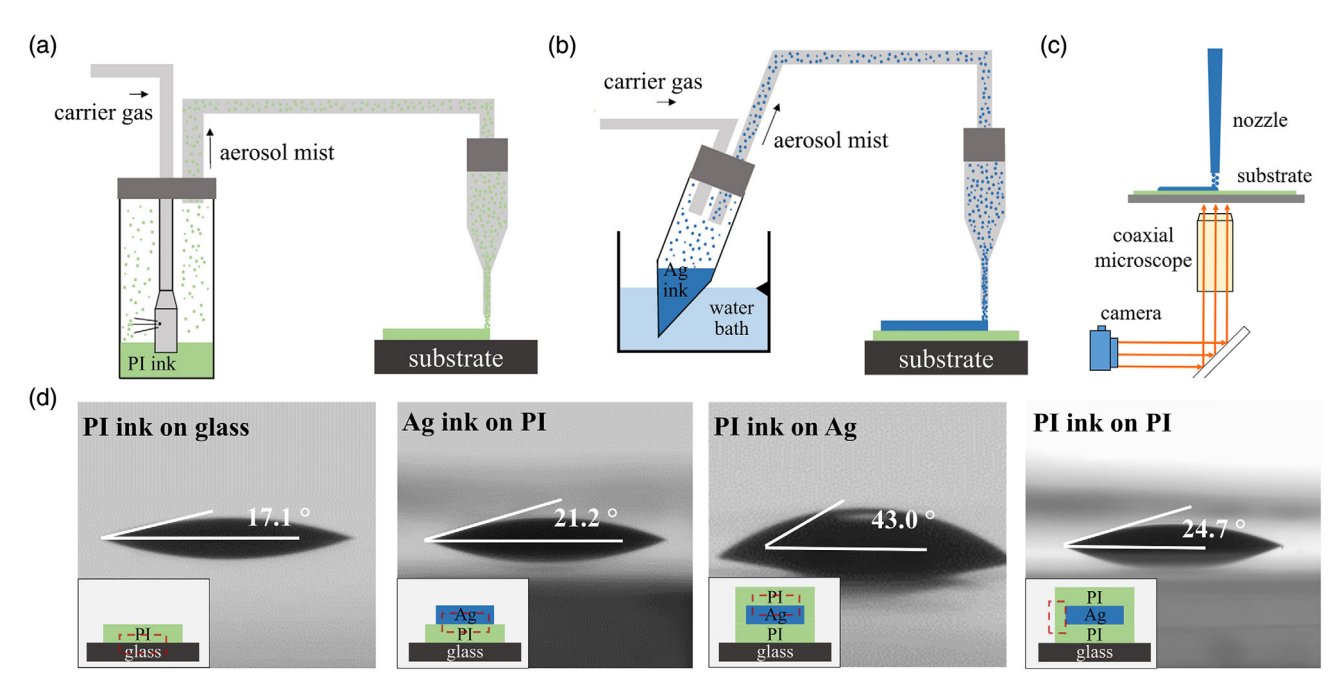


Figure 2. Schematics of aerosol printing with a) Collison nebulizer for PI ink, b) ultrasonic particle generator for Ag ink, and c) bottom-view coaxial microscope for alignment. d) Contact angle measurement results for PI ink and Ag ink printed on the substrate and previously deposited layers during the layer-by-layer process.

of the sandwich-structured conductors was highly dependent on the wetting behaviors of the droplets of the printable inks of PI and Ag on the substrate, as well as the layers of the previously deposited materials. Hence, contact angle measurements were carried out for these cases to validate the layer-by-layer printing process. The images showing the morphology of the stabilized ink droplets and the results of measured contact angles are shown in Figure 2d. For all cases, the contact angles were smaller than 45°, indicating the hydrophilic wetting behaviors of the droplets of both PI ink and Ag ink on the substrate and the previously printed layers without any surface treatment. The hydrophilic wetting behaviors were essential for the successful printing, as the landed microdroplets would stay and coalesce into the designed patterns.

Figure 3a–c shows the optical microscopic images of the line morphology of the printed PI layer, Ag layer, and the sandwich-structured conductors. As shown in images, both PI and Ag inks were printable into dense and uniform lines. Overspray of splattered aerosol microdroplets was observed for both cases as the typical feature of aerosol printed materials. To avoid potential issues such as short circuit caused by the overspray, the PI layers had to be intentionally printed wider than the Ag layers to ensure the full coverage of encapsulated Ag layers. As shown in Figure 3c, the printed PI and Ag layers were well aligned into the sandwich-structured conductors with the Ag layer fully encapsulated.

The linewidths of the printed PI and Ag layers were measured with varied printing speed and the results are plotted in Figure 3d. The optical microscopic images showing the line morphology of the printed PI layers and Ag layers with varied printing speeds are shown in Figure S1 and Figure S2. The

relationship between the linewidth and the electrical resistance of the Ag layers with the varied printing speed is shown in Figure S2e. For all cases of printing speed, the linewidth of PI layers was always bigger than that of Ag layers. It was also observed that with increased printing speed, the width of the overspray region became more significant compared with the linewidth for both PI and Ag layers. For this reason, a relatively low printing speed of 0.5 mm s $^{-1}$ was chosen for both PI and Ag layers in the sandwich-structured conductors. The thickness of the printed PI and Ag layers by speed of 0.5 mm s $^{-1}$ was measured to be $0.78\pm0.4\,\mu m$ and $0.97\pm0.7\,\mu m$, respectively (Figure S3).

It is already known that during the postprocess annealing, a high annealing temperature would facilitate the sintering process of the printed Ag NPs, in which the separated NPs start to grow and form necking connections with their neighboring NPs. These connections serve as the pathway for the transportation of electrons and contribute to the electronic conductivity of the Ag layer. To understand the effect of postprocess annealing of the sandwich-structured conductors, the microstructures of the Ag layers were examined by scanning electron microscopy (SEM). As mentioned previously, the first annealing and second annealing steps are referred to those applied after printing of Ag layer (to the PI/Ag two-layer structure, at temperatures varying from 150 °C to 250 °C) and after printing of the top PI layer (to the PI/Ag/PI sandwich structure, at a fixed temperature of 250 °C as needed for the imidization of the top PI layer), respectively. As shown in the SEM images, compared with the unannealed Ag layer (Figure 4a), significant grain growth of the Ag NPs was observed after the first annealing (Figure 4b) even at a low temperature of 150 °C. Both individual NPs and NPs with www.advancedsciencenews.com www.aem-journal.com

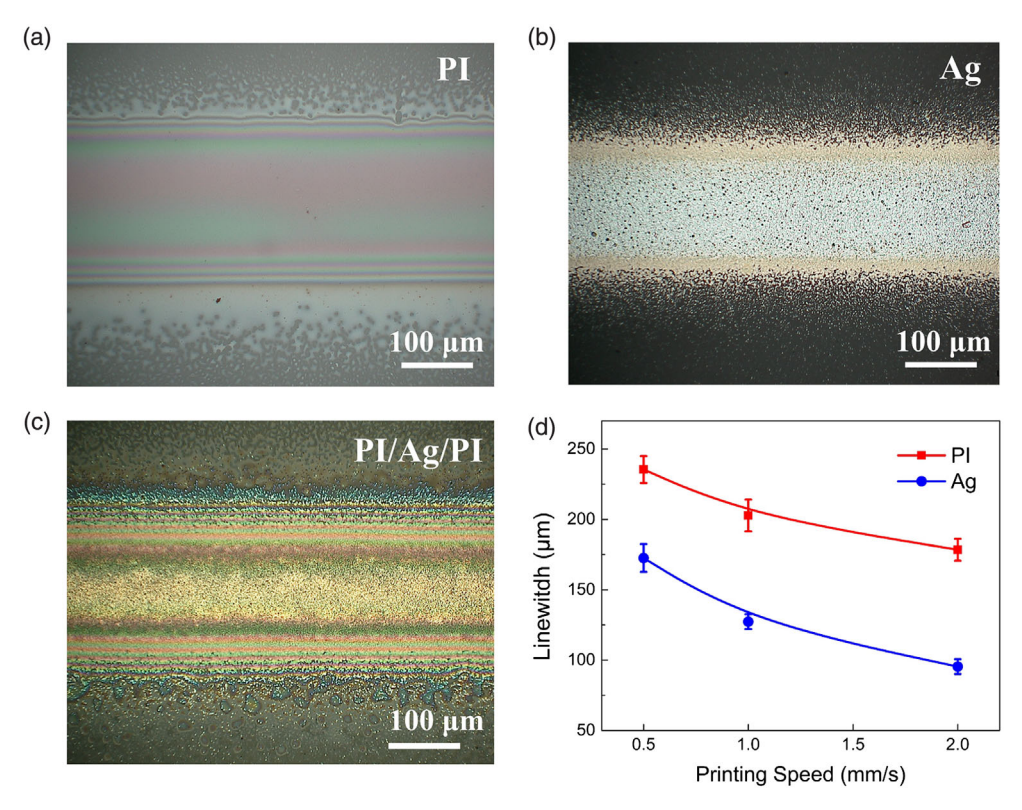


Figure 3. Optical microscopic images showing the line morphology of a) PI layer, b) Ag layer, and c) PI/Ag/PI sandwich-structured conductor. d) Effect of printing speed on the linewidth of the PI and Ag layers.

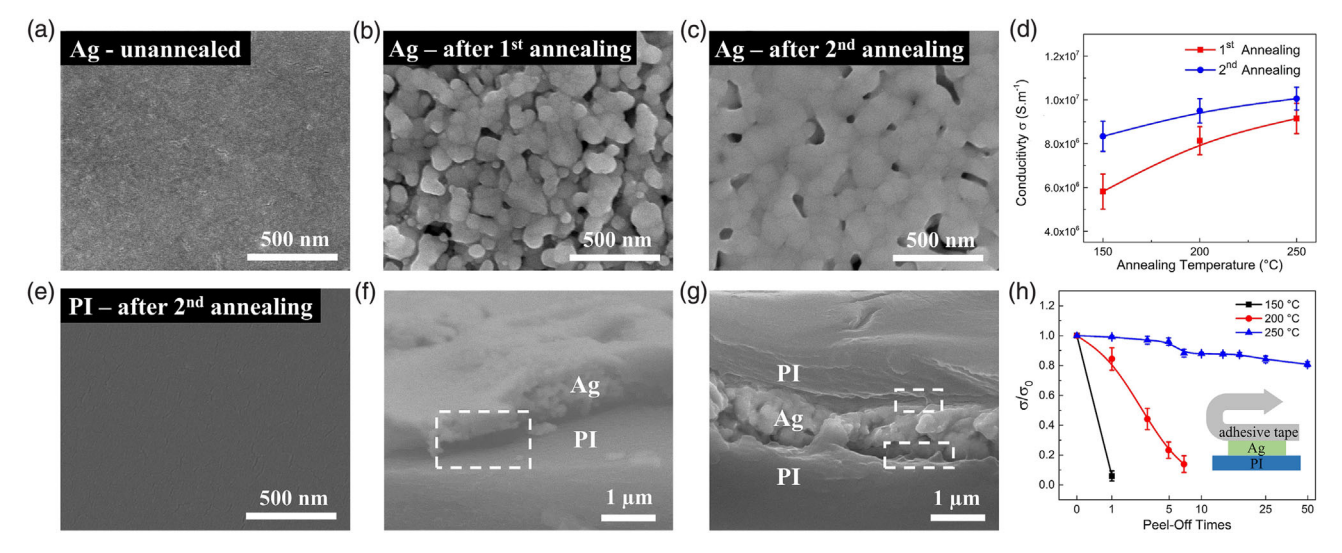


Figure 4. SEM images of the as-printed Ag layers a) before annealing, b) after first annealing at 150 °C, and c) after second annealing. d) Effect of temperature used in the first annealing on the electronic conductivity of the Ag layers. e) SEM image of the PI layer after second annealing. f) Cross-section SEM images of the PI/Ag two-layer structure after first annealing at 150 °C and g) the PI/Ag/PI sandwich structure after second annealing. h) Conductivity loss of the Ag layers with different annealing temperatures in the peel-off test.

necking connections formed with their neighboring NPs are shown in Figure 4b, indicating that the sintering process had started but was not sufficient. After the second annealing (Figure 4c), further development in the grain size of the Ag NPs occurred. Moreover, the NPs were all connected with their

neighboring NPs without any individual NPs observed, suggesting the substantial growth of the conductive networks in the Ag layer.

To further investigate the effect of annealing temperature, electronic conductivity of the Ag layers was examined after both





www.aem-journal.com

first annealing and second annealing. As shown in Figure 4d, the electronic conductivity of the Ag layers was positively dependent on the annealing temperature. After the first annealing, the conductivity of Ag layers ranged from 5.8×10^6 S m⁻¹ to 9.2×10^6 S m⁻¹ with annealing temperature increasing from 150 °C to 250 °C. A series of SEM images showing the microstructures of the Ag layers after first annealing under 150 °C, 200 °C, and 250 °C is shown in Figure S4, which reveals the growth of conductive networks in the Ag layers with increased annealing temperature. After the second annealing, the electronic conductivity of Ag layers was further enhanced for all cases. The increase in conductivity was most significant for Ag layer annealed at 150 °C during the first annealing, from 5.8×10^6 S m⁻¹ to 8.3×10^6 S m⁻¹. The conductivity of Ag layer annealed at 250 °C was further increased to 1.14×10^7 S m⁻¹, which was in the same order of magnitude to the conductivity of bulk silver at 6.3×10^7 S m⁻¹. The obtained electronic conductivity was sufficiently high sandwich-structured conductors to serve as the contacts and interconnects for most applications.

The microstructure of the PI layer was also examined by SEM (Figure 4e). The PI layer had a smooth surface, which helped the continuous deposition of the subsequently printed layers. In addition, the interfaces of the PI and Ag layers were examined by cross-section SEM. In the cross-section SEM image of the PI/ Ag two-layer structure after first annealing at 150 °C (Figure 4f), the delamination of the Ag layer from the PI layer was observed (marked in the dashed rectangle). The delamination could have come from the SEM sample preparation; however, it still indicated a weak interfacial bonding between the PI and Ag layers. However, after the second annealing (Figure 4g), the PI/Ag/PI sandwich structure exhibited integrity at both bottom PI/Ag and Ag/top PI interfaces. In both bottom and top PI layers, some tiny tip-shaped structures (marked in the dashed rectangle) were observed, which were very likely to be formed during the second annealing at a high temperature of 250 °C. Such structures as the evidence of interfacial fusion could contribute to the improved interfacial bonding between the PI and Ag layers.

Peel-off test was conducted to evaluate the effect of annealing temperature on the interfacial bonding between the PI and Ag layers. The Ag layers were printed on the spin-coated and preannealed PI films, followed by annealing at 150 °C, 200 °C, or 250 °C. Adhesive tape was applied on and then peeled off from the surface of the Ag layer for one time of peel-off. The peel-off process was repeated multiple times to evaluate the interfacial bonding between the Ag and PI layers. The conductivity loss of the Ag layers as a function of peel-off times is plotted in Figure 4h. The Ag layers annealed at 150 °C exhibited a huge loss in electronic conductivity immediately after the first peel-off. The Ag layers annealed at 200 °C survived the first several peel-offs. However, it lost most of the conductivity after peeling off eight times. The Ag layers annealed at 250 °C were able to retain most of the electronic conductivity during the peel-off test, with a retention of 81% in the electronic conductivity after peeling off for 50 times. The results of the peel-off test indicated that increased annealing temperature significantly improved the interfacial bonding between the PI and Ag layers.

The sandwich-structured conductors were transferrable to various plastic substrates through a thiol—epoxy bonding process

for application in flexible electronics. The bonding process was validated through the peel test between PI film and different substrates (Figure S5 and Table S2). The cross-section SEM image of the PI/Ag/PI sandwich structure is shown in Figure S6. Several example devices were fabricated to demonstrate the application. Figure 5a shows the photograph of a spiral-shaped sandwich-structured conductor on the PS substrate and Figure 5b shows an light-emitting diode (LED) circuit with the sandwich-structured conductor on the PET substrate. In addition, a five-layer capacitor (Figure 5c), consisting of bottom and top PI encapsulating layers, two Ag electrode layers, and a PI dielectric layer, was fabricated and transferred to a Kapton film. Figure 4d shows the optical microscopic image of the five-layer capacitor with the cross-section view of the layer design shown in the inset. The five-layer capacitor was used together with a carbon black (CB) resistor (Figure S7a) as a high-pass filter. The bode plot of the high-pass filter in Figure 5e demonstrated its functionality. The five-layer capacitor was also studied with a varied printing area. The results in Figure S7b-d show that the printed five-layer capacitor with tunable capacitance values could serve for different signal processing purposes.

Bending test was conducted to investigate the mechanical robustness of the flexible sandwich-structured conductors transferred to Kapton film (T-3L). Their electronic conductivity was examined under bending deformation and compared with the conductors directly printed on Kapton film (DP) and the transferred PI/Ag two-layer conductors (T-2L). The conductivity losses of these three types of conductors during bending test are plotted in Figure 5f. The length of the fixture at the two ends of the substrate L was adjusted with reduced length ΔL to realize the bending. The reduced length ratio $\Delta L/L$ of 0, 0.1, 0.2, 0.3, and 0.4 corresponded to the radius of curvature from infinite to 9.33, 6.59, 5.38, and 4.66 mm. At $\Delta L/L = 0.4$, the loss of electronic conductivity for DP, T-2L, and T-3L conductors was 23%, 13%, and 5%, respectively. In addition, after the bent conductors were released to flat status, the recovered electronic conductivity was also measured and shown as the datapoints with hollow symbols at $\Delta L/L = 0$ in Figure 5f. The T-3L conductors were found to have much less conductivity loss compared with DP and T-2L conductors with nearly fully recovered electronic conductivity (\approx 99.8%) upon release. The conductivity loss of the T-3L conductors during cyclic bending is plotted in Figure S8a, indicating the good operational stability of the flexible sandwich-structured conductors.

Besides the flexible plastic substrates, the sandwich-structured conductors were also transferred to elastomeric PDMS substrate for application in stretchable electronics. The sandwich-structured conductors were printed with two different geometric designs in straight line and serpentine line and their conductivity loss during the stretching test was investigated. Similar to the bending test, the length of the fixture at the two ends of the substrate L was adjusted with elongated length ΔL to realize the stretching. As shown in Figure 5g, for sandwich-structured conductors printed in straight line and serpentine line, the retention of electronic conductivity was as high as 98.7% and 99.5% with elongated length ratio $\Delta L/L$ at 0.4 and 0.6 (strain at 40% and 60%). The conductivity loss of the stretchable sandwich-structured conductors in serpentine line during cyclic stretching is plotted in Figure S8b. The

www.advancedsciencenews.com www.aem-journal.com

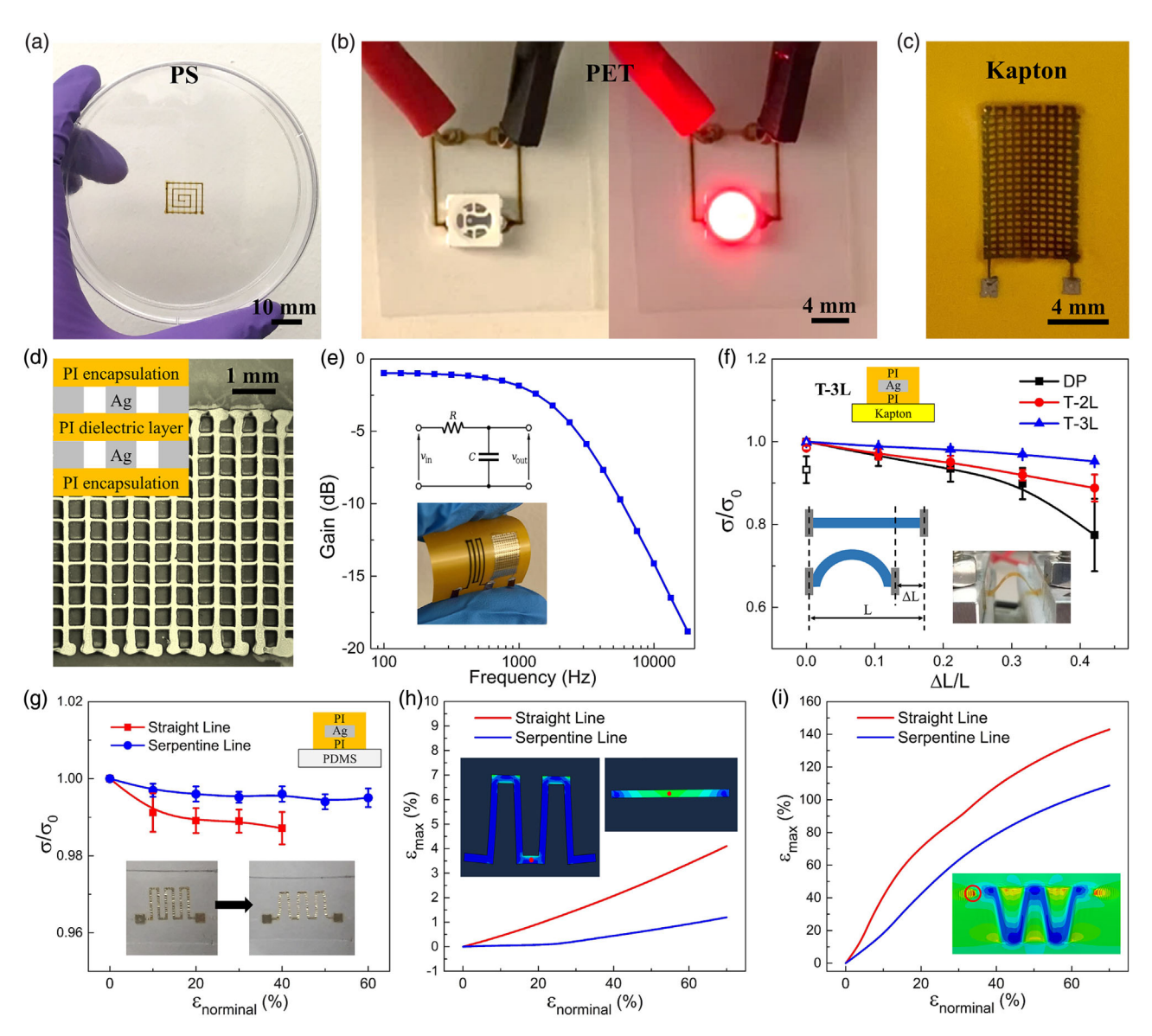


Figure 5. a) Photograph of the spiral-shaped sandwich-structured conductor on PS substrate. b) Photograph of LED circuit with the sandwich-structured conductor on PET substrate. c) Photograph of five-layer capacitor on Kapton thin film. d) Optical microscopic image of the five-layer capacitor with the inset showing the cross-section view of the layer design. e) Bode plot of the high-pass filter with the five-layer capacitor and CB resistor. f) Conductivity loss of the transferred flexible sandwich-structured conductors (T-3L) compared with transferred two-layer PI/Ag conductors (T-2L) and DP conductors in the bending test. g) Conductivity loss of the stretchable sandwich-structured conductors with straight-line and serpentine-line geometric designs in the stretching test. h) FEA results of the maximum first-principal strain ε_{max} in the central element of the conductor and i) in the PDMS element nearest to the end of the conductor during stretching.

negligible conductivity loss revealed the mechanical robustness and operational stability of the sandwich-structured conductors themselves during stretching and demonstrated their potential application in stretchable electronics.

Nevertheless, mechanical failures either in the substrate or at the interface between the conductor and substrate were observed for the straight line and serpentine line during stretching. As shown in Figure S9a, the sandwich-structured conductor in straight line had the PDMS substrate with cohesive failure at the location nearest to the end of the conductor with strain > 40%. Figure S9b shows the delaminating corners of the sandwich-structured conductor in serpentine line from the PDMS substrate with strain > 60%.

To better understand the strain distribution in the sandwich-structured conductors and the substrates during stretching, as well as to explore the underlying mechanisms of the observed mechanical failures, finite-element analysis (FEA) was conducted to simulate the stretching process of the sandwich-structured conductors on PDMS substrates. The results of maximum first-principal strain $\varepsilon_{\rm max}$ in the central element of the conductor





www.aem-journal.com

(marked as red dots in the insets of Figure 5h) and in the PDMS element nearest to the end of the conductor during stretching (marked as red circle in the inset of Figure 5i) are plotted in Figure 5h and i. The $\varepsilon_{\mathrm{max}}$ of the central element of the sandwich-structured conductors was much smaller in the serpentine line compared with the straight line, indicating that the geometric design of serpentine line helped in the stretchability of the sandwich-structured conductors. Furthermore, higher ε_{\max} of the PDMS element in the straight line could account for the cohesive failure of PDMS substrate (Figure S9a) observed during the stretching test. In addition, $\varepsilon_{\rm max}$ of various local elements of the sandwichstructured conductors was compared for both straight-line and serpentine-line cases, as shown in Figure S10, which further revealed the potential cause of the delaminating corners (Figure S9b) of the sandwich-structured conductors in serpentine line from the PDMS substrate. Based on the FEA results, improvement on the stretchable sandwich-structured conductors could be made in future works in the aspects of 1) utilizing substrates with better stretchability such as Ecoflex^[47] and polyurethane, ^[48] 2) enhancing the interfacial bonding between the conductors and the elastomeric substrate, 3) improving the geometric design to optimize the dimensional parameters or using designs with better stretchability such as the horseshoe structure. [49,50]

3. Conclusion

In summary, additive manufacturing of highly conductive, sandwich-structured NP-based conductors as a potential route for the fabrication of conductors in flexible and stretchable electronics with high-temperature processibility and versatility in applicable substrates was successful demonstrated. The feasibility of layer-by-layer printing was validated with the hydrophilic wetting behaviors of the printable inks on the substrate, as well as the layers of the previously deposited materials. The postprocess annealing of the as-printed sandwich-structured conductors was found to significantly contribute to the growth of conductive networks in the printed Ag layer. The Ag layer annealed at 250 °C exhibited high electronic conductivity of 1.14×10^7 S m⁻¹, which was in the same order of magnitude to the conductivity of bulk silver at 6.3×10^7 S m⁻¹ and was sufficiently high for serving as the contacts and interconnects in most applications. In addition, a high annealing temperature of 250° also contributed to the significantly improved interfacial bonding between the Ag and PI layers. The printed conductors were transferrable to various substrates through a thiol-epoxy bonding process, including PS, PET, Kapton, and PDMS thin films for applications in flexible and stretchable electronics with example devices such as LED circuit and five-layer capacitor to demonstrate the applications. The flexible sandwich-structured conductors transferred to Kapton substrates were found to have much less conductivity loss compared with DP conductors during the bending test. The stretchable sandwich-structured conductors transferred to PDMS elastomeric substrate exhibited negligible conductivity loss with strain up to 60%. FEA revealed the strain distribution in the stretchable sandwich-structured conductors and the substrates during stretching and also provided future directions to optimize the sandwich-structured conductors for application in stretchable electronics.

4. Experimental Section

Ink Preparation, Aerosol Printing, and Postprocess Annealing of the PI/Ag/ PI Sandwich-Structured Conductors: PI ink was obtained by diluting a polyamic acid solution (HD Microsystem PI-2545) with 1-methyl-2pyrrolidinone (NMP, Sigma-Aldrich) in the weight ratio of 1:1. The as-prepared PI ink was atomized with a Collison nebulizer. Nitrogen was used as the carrier gas and PI ink was printed with gas flow rate of 0.4 LPM on a glass slide as the bottom PI layer. The bottom PI layer was preannealed at 250 °C for 1 h for imidization. Ag ink was purchased from UT Dots, Inc. (UTDAg40X). It was atomized with an ultrasonic particle generator with the transducer power was set to 40%. Nitrogen was used as the carrier gas and the Ag ink was printed with gas flow rate of 35 sccm on the previously printed bottom PI layer. The printed Ag was annealed at different temperatures from 150 °C to 250 °C for 1 h as the first annealing step. Another PI layer was printed with the same procedure onto the previously printed Ag layer as the top PI layer. After printing the top PI layer, it also needed to be heat treated for imidization, so the whole PI/Ag/PI sandwich structure was annealed at 250 °C for 1 h as the second annealing step. During layer-by-layer printing, a bottom-view coaxial microscope was used to ensure the alignment of each layer. Printing patterns for the top PI layer were the same as the bottom PI layer and the Ag layer except that they did not cover the contact pads at the two ends of the patterns.

Characterization of the Printed Sandwich–Structured Conductors: The wetting behaviors of the printable inks were characterized by a contact angle measurement system (DataPhysics OCA 15EC). The line morphology of the printed PI layer, Ag layer, and the sandwich-structured conductors was observed by an optical digital microscope (Hirox KH-8700) and the linewidth with different printing speeds was measured accordingly. The microstructures of the sandwich-structured conductors were observed by SEM (Hitachi S-4700). Electronic conductivity was measured with probing tips on the printed contact pads by a digital multimeter (Tektronix DMM4050).

Substrate-Transferring Process with Thiol-Epoxy Bonding: The sandwichstructured conductors printed on the glass slide as donor substrate were picked up by a water-soluble tape (Aquasol Corp.) as the intermediate substrate. A PVA-based water-soluble glue was spin coated at 500 rpm onto the donor substrate prior to the lamination of the water-soluble tape to enhance adhesion. The thiol-epoxy bonding process was conducted by first treating both the target substrate and the sandwich-structured conductors (at the bottom PI layer) with oxygen plasma (Plasma Etch PE-200) and then immersed in a 1% v/v solution of (3-mercaptopropyl) trimethoxysilane (MPTMS, Sigma-Aldrich) and (3-glycidyloxypropyl) trimethoxysilane (GPTMS, Sigma-Aldrich) in methanol for 1 h. After the treatment, they were pressed into conformal contact and left overnight at room temperature (for PDMS) or at 80 °C (for other target substrates) to allow the formation of thiol-epoxy bonding. The sandwich-structured conductors on the target substrate were immersed in DI water for 1 h to ensure the full removal of water-soluble tape and PVA-based glue and then

FEA of the Stretchable Sandwich–Structured Conductors: The commercial FEA software Abaqus was used to simulate the stretching process of stretchable sandwich-structured conductors. The whole sandwich-structured conductor was assumed as one layer given the good interfacial bonding between the Ag and PI layers. Perfect adhesion was assumed between the sandwich-structured conductors and the elastomeric substrate PDMS. Neo–Hookean hyperelastic material model^[51] (Young's modulus = 0.6 MPa) and linear elastic material model^[52–54] (Young's modulus = 9.2 GPa and Poisson's ratio = 0.34) were used for PDMS and sandwichstructured conductors, respectively.

Supporting Information

Supporting Information is available from the Wiley Online Library or from the author.



www.aem-journal.com

ENGINEERING

Acknowledgements

This work is supported by seed fund from Intelligent System Center (ISC) at Missouri University of Science and Technology. This work is also partially supported by the National Science Foundation under grant No. 1635256 and No. 1846673. The financial supports are greatly appreciated. The authors would like to thank Dr. Eric Bohannan and Dr. Clarissa Wisner for their help in material characterizations.

Conflict of Interest

The authors declare no conflict of interest.

Data Availability Statement

Research data are not shared.

Keywords

additive manufacturing, aerosol printing, conductors, flexible electronics, polyimide, printed electronics, stretchable electronics

Received: March 9, 2021 Revised: June 21, 2021 Published online:

- T. Sekitani, Y. Noguchi, K. Hata, T. Fukushima, T. Aida, T. Someya, Science 2008, 321, 1468.
- [2] J. A. Rogers, T. Someya, Y. Huang, Science 2010, 327, 1603.
- [3] X. Huang, W. H. Yeo, Y. Liu, J. A. Rogers, Biointerphases 2012, 7, 52.
- [4] G.-W. Huang, H.-M. Xiao, S.-Y. Fu, Sci. Rep. 2015, 5, 13971.
- [5] J. C. Yeo, H. K. Yap, W. Xi, Z. Wang, C.-H. Yeow, C. T. Lim, Adv. Mater. Technol. 2016, 1, 1600018.
- [6] S. Yao, J. Cui, Z. Cui, Y. Zhu, Nanoscale 2017, 9, 3797.
- [7] S. J. Kim, K. W. Cho, H. R. Cho, L. Wang, S. Y. Park, S. E. Lee, T. Hyeon, N. Lu, S. H. Choi, D.-H. Kim, Adv. Funct. Mater. 2016, 26 3207
- [8] W.-H. Yeo, Y.-S. Kim, J. Lee, A. Ameen, L. Shi, M. Li, S. Wang, R. Ma, S. H. Jin, Z. Kang, Y. Huang, J. A. Rogers, Adv. Mater. 2013, 25, 2773.
- [9] R. F. Pease, S. Y. Chou, Proc. IEEE 2008, 96, 248.
- [10] X. Yu, K. B. Mahajan, W. Shou, H. Pan, Micromachines 2017, 8, 7.
- [11] S. H. Ko, H. Pan, C. P. Grigoropoulos, J. M. J. Fréchet, C. K. Luscombe, D. Poulikakos, Appl. Phys. A Mater. Sci. Process. 2008, 92, 579.
- [12] T. Vuorinen, J. Niittynen, T. Kankkunen, T. M. Kraft, M. Mäntysalo, Sci. Rep. 2016, 6, 35289.
- [13] D. Zhao, T. Liu, J. G. Park, M. Zhang, J.-M. Chen, B. Wang, Microelectron. Eng. 2012, 96, 71.
- [14] K. Wang, Y.-H. Chang, C. Zhang, B. Wang, Carbon N. Y. 2016, 98, 397.
- [15] X. Yu, Y. Liu, H. Pham, S. Sarkar, B. Ludwig, I. M. Chen, W. Everhart, J. Park, Y. Wang, H. Pan, Adv. Mater. Technol. 2019, 4, 1900645.
- [16] B. K. Mahajan, B. Ludwig, W. Shou, X. Yu, E. Fregene, H. Xu, H. Pan, X. Huang, Sci. China Inf. Sci. 2018, 61, 60412.
- [17] Y. Han, J. Dong, Adv. Mater. Technol. 2017, 3, 1700268.
- [18] Z. Cui, Y. Han, Q. Huang, J. Dong, Y. Zhu, Nanoscale 2018, 10, 6806.
- [19] E. Jabari, E. Toyserkani, Carbon N. Y. 2015, 91, 321.

- [20] K. Kordás, T. Mustonen, G. Tóth, H. Jantunen, M. Lajunen, C. Soldano, S. Talapatra, S. Kar, R. Vajtai, P. M. Ajayan, Small 2006, 2, 1021.
- [21] Y. Y. Lee, H. Y. Kang, S. H. Gwon, G. M. Choi, S. M. Lim, J. Y. Sun, Y. C. Joo, Adv. Mater. 2016, 28, 1636.
- [22] A. Kamyshny, Open Appl. Phys. J. 2011, 4, 19.
- [23] K. S. Bhat, R. Ahmad, Y. Wang, Y. B. Hahn, J. Mater. Chem. C 2016, 4, 8522
- [24] D. Kim, S. Jeong, J. Moon, K. Kang, Mol. Cryst. Liq. Cryst. 2006, 459, 45.
- [25] L. Mo, Z. Guo, Z. Wang, L. Yang, Y. Fang, Z. Xin, X. Li, Y. Chen, M. Cao, Q. Zhang, L. Li, *Nanoscale Res. Lett.* 2019, 14, 197.
- [26] T. Seifert, E. Sowade, F. Roscher, M. Wiemer, T. Gessner, R. R. Baumann, Ind. Eng. Chem. Res. 2015, 54, 769.
- [27] T. T. Nge, M. Nogi, K. Suganuma, J. Mater. Chem. C 2013, 1, 5235.
- [28] S. H. Ko, Semicond. Sci. Technol. 2016, 31, 73003.
- [29] C. Kim, M. Nogi, K. Suganuma, Y. Yamato, ACS Appl. Mater. Interfaces 2012, 4, 2168.
- [30] S. Jeong, H. C. Song, W. W. Lee, Y. Choi, B. H. Ryu, J. Appl. Phys. 2010, 108, 102805.
- [31] H. Kang, E. Sowade, R. R. Baumann, ACS Appl. Mater. Interfaces 2014, 6. 1682.
- [32] C. N. Chen, C. P. Chen, T. Y. Dong, T. C. Chang, M. C. Chen, H. T. Chen, I. G. Chen, Acta Mater. 2012, 60, 5914.
- [33] K. C. Yung, X. Gu, C. P. Lee, H. S. Choy, J. Mater. Process. Technol. 2010, 210, 2268.
- [34] X. Nie, H. Wang, J. Zou, Appl. Surf. Sci. 2012, 261, 554.
- [35] M.-T. Lee, D. Lee, A. Sherry, C. P. Grigoropoulos, J. Micromech. Microeng. 2011, 21, 95018.
- [36] J. Wu, R. C. Roberts, N. C. Tien, D. Li, Sensors, 2014 IEEE 2014, 1100.
- [37] Y. Kim, X. Ren, J. W. Kim, H. Noh, J. Micromech. Microeng. 2014, 24, 115010.
- [38] J. Sun, J. Jiang, B. Bao, S. Wang, M. He, X. Zhang, Y. Song, *Materials (Basel)* 2016, 9, 253.
- [39] J. Abu-Khalaf, L. Al-Ghussain, A. Nadi, R. Saraireh, A. Rabayah, S. Altarazi, A. Al-Halhouli, *Materials (Basel)* 2019, 12.
- [40] S. Agarwala, G. L. Goh, T. S. Dinh Le, J. An, Z. K. Peh, W. Y. Yeong, Y. J. Kim, ACS Sensors 2019, 4, 218.
- [41] J. N. Lee, C. Park, G. M. Whitesides, Anal. Chem. 2003, 75, 6544.
- [42] R. Dangla, F. Gallaire, C. N. Baroud, Lab Chip 2010, 10, 2972.
- [43] L. Tang, N. Y. Lee, Lab Chip 2010, 10, 1274.
- [44] M. V. Hoang, H.-J. Chung, A. L. Elias, J. Micromech. Microeng. 2016, 26, 105019.
- [45] G. Chen, Y. Gu, H. Tsang, D. R. Hines, S. Das, Adv. Eng. Mater. 2018, 20, 1701084.
- [46] A. Mahajan, C. D. Frisbie, L. F. Francis, ACS Appl. Mater. Interfaces 2013, 5, 4856.
- [47] J. Yun, Y. Lim, G. N. Jang, D. Kim, S.-J. Lee, H. Park, S. Y. Hong, G. Lee, G. Zi, J. S. Ha, Nano Energy 2016, 19, 401.
- [48] W. Hu, X. Niu, R. Zhao, Q. Pei, Appl. Phys. Lett. 2013, 102, 83303.
- [49] M. Gonzalez, F. Axisa, M. Vanden Bulcke, D. Brosteaux, B. Vandevelde, J. Vanfleteren, *Microelectron. Reliab.* 2008, 48, 825.
- [50] Q. Jing, Y. S. Choi, M. Smith, C. Ou, T. Busolo, S. Kar-Narayan, Adv. Mater. Technol. 2019, 4, 1900048.
- [51] Y. Wang, Z. Yu, G. Mao, Y. Liu, G. Liu, J. Shang, S. Qu, Q. Chen, R. W. Li, Adv. Mater. Technol. 2019, 4, 1800435.
- [52] L. Guo, G. S. Guvanasen, X. Liu, C. Tuthill, T. R. Nichols, S. P. Deweerth, IEEE Trans. Biomed. Circuits Syst. 2013, 7, 1.
- [53] J. Y. Sun, N. Lu, J. Yoon, K. H. Oh, Z. Suo, J. J. Vlassak, J. Mater. Res. 2009, 24, 3338.
- [54] J. Pu, X. Wang, R. Xu, S. Xu, K. Komvopoulos, *Microsyst. Nanoeng.* 2018, 4, 1.